Enhancement of secondary organic aerosol formation and its oxidation state by SO_2 during photooxidation of 2-methoxyphenol

Changgeng Liu[1,2,a], Tianzeng Chen[1,4,a], Yongchun Liu[3], Jun Liu[1,4], Hong He[1,4,5], Peng Zhang[1,4]

[1]State Key Joint Laboratory of Environment Simulation and Pollution Control, Research Center for Eco-Environmental Sciences, Chinese Academy of Sciences, Beijing 100085, China

[2]School of Biological and Chemical Engineering, Panzhihua University, Panzhihua 617000, China

[3]Beijing Advanced Innovation Center for Soft Matter Science and Engineering, Beijing University of Chemical Technology, Beijing 100029, China

[4]University of Chinese Academy of Sciences, Beijing 100049, China

[5]Center for Excellence in Regional Atmospheric Environment, Institute of Urban Environment, Chinese Academy of Sciences, Xiamen 361021, China

[a]These authors contributed equally to this work and should be considered as co-first authors

Correspondence to: Yongchun Liu (liuyc@buct.edu.cn) and Hong He (honghe@rcees.ac.cn)

Abstract. 2-Methoxyphenol (guaiacol) is derived from the lignin pyrolysis and taken as a potential tracer for wood smoke emissions. In this work, the effect of SO_2 at atmospheric levels (0−56 ppbv) on secondary organic aerosol (SOA) formation and its oxidation state during guaiacol photooxidation was investigated in the presence of various inorganic seed particles (i.e., NaCl and $(NH_4)_2SO_4$). Without SO_2 and seed particles, SOA yields ranged from (9.46 ± 1.71) % to (26.37 ± 2.83) % and could be well expressed by a one-product model. According to the ratio of the average gas-particle partitioning timescale ($\overline{\tau}_{g\text{-}p}$) over the course of experiment to the vapor wall deposition timescale ($\tau_{g\text{-}w}$), the determined SOA yields were underestimated by a factor of ~2 times. The presence of SO_2 resulted in enhancing SOA yield by 14.04 %−23.65 %. With $(NH_4)_2SO_4$ and NaCl seed particles, SOA yield was enhanced by 23.07 % and 29.57 %, respectively, which further increased significantly to 29.78 %−53.43 % in the presence of SO_2, suggesting that SO_2 and seed particles have a synergetic contribution to SOA formation. The decreasing trend of $\overline{\tau}_{g\text{-}p} / \tau_{g\text{-}w}$ ratio in the presence of seed particles and SO_2 suggested that more SOA-forming vapors were partitioned onto particle phase, consequently increasing SOA yields. It should be noted that SO_2 was found to be in favor of increasing the carbon oxidation state (OS_C) of SOA, indicating that the functionalization reaction or the partitioning of highly oxidized products onto particles should be more dominant than oligomerization reaction. In addition, the average N/C ratio of SOA was 0.037, which revealed that NO_x participated in the photooxidation process, consequently leading to the formation of organic N-containing

compounds. The experimental results demonstrate the importance of SO_2 on the formation processes of SOA and organic S-containing compounds, and also are helpful to further understand SOA formation from the atmospheric photooxidation of guaiacol and its subsequent impacts on air quality and climate.

1 Introduction

Biomass burning is considered as one of the major sources of gas and particulate pollutants in the atmosphere (Lauraguais et al., 2014b; Yang et al., 2016). Therefore, it has significant adverse impacts on regional and global air quality (Bari and Kindzierski, 2016; Lelieveld et al., 2001), climate (Chen and Bond, 2010), and human health (Naeher et al., 2007). The chemical species emitted by biomass burning is mainly dependent on fuel source and combustion conditions (O'Neill et al., 2014). Natural wood is composed of cellulose (40−50 wt.%), hemicelluloses (25−35 wt.%), and lignin (18−35 wt.%) (Nolte et al., 2001). During the burning process, lignin pyrolysis could result in the formation of methoxyphenols, mainly including guaiacol (2-methoxyphenol), syringol (2,6-dimethoxyphenol), and their derivatives (Nolte et al., 2001; Schauer et al., 2001). Due to the high emission rate of methoxyphenols (900−4200 mg kg^{-1} wood), methoxyphenols are considered as the potential tracers for wood burning (Hawthorne et al., 1989, 1992; Simoneit et al., 1993).

As a representative type of methoxyphenols, guaiacol mainly exists in the gas phase and is widely found in the atmosphere (Schauer et al., 2001). Its emission factor of wood burning is in the range of 172−279 mg kg^{-1} wood (Schauer et al., 2001). In recent years, the reactivity of gas-phase guaiacol toward OH radicals (Coeur-Tourneur et al., 2010a), NO_3 radicals (Lauraguais et al., 2016; Yang et al., 2016), Cl atom (Lauraguais et al., 2014a), and O_3 (El Zein et al., 2015) has been investigated, suggesting that its degradation by OH and NO_3 radicals might be predominant in the atmosphere.

Meanwhile, several studies have reported the significant SOA formation from guaiacol oxidation by OH radicals, produced from the photolysis of the OH precursors (i.e., H_2O_2 and CH_3ONO) (Ahmad et al., 2017; Lauraguais et al., 2014b; Yee et al., 2013). However, SOA formation from the photooxidation of guaiacol in the presence of NO_x has not been investigated without adding the direct OH precursor, even though it has been recently reported that the atmospheric level of NO_x could reach up to close 200 ppbv in the severely polluted climate in China (Li et al., 2017).

Although many studies concentrated on the SOA production from the oxidation of volatile organic compounds (VOCs), the reported SOA yields showed high variability for a given precursor (Chu et al., 2016, 2017; Ge et al., 2017a; Lauraguais et al., 2012, 2014b; Ng et al., 2007; Sarrafzadeh et al., 2016; Yee et al., 2013). This variability is mainly dependent on the numerous factors, e.g., pre-existing seed particles, SO_2 level, NO_x level, humidity, and temperature. Two of the critical factors are the impacts of pre-existing seed particles and SO_2 level on SOA formation (Chu et al., 2016, 2017; Ge et al., 2017a). In addition, the atmospheric concentration of SO_2 could be up to close 200 ppbv in the severely polluted atmosphere in China, and SOA from biomass burning and sulfate formation could significantly contribute to severe haze pollution (Li et al., 2017). During the transport process, smoke plumes from biomass burning would be inevitably mixed with suspended particles (e.g., $(NH_4)_2SO_4$ particles), SO_2, and NO_x in the atmosphere. However, the influences of these co-existed pollutants on the transformation of guaiacol and its SOA formation are still unclear. For these reasons,

the aim of this work was to investigate the SOA formation from guaiacol photooxidation in the presence of NO_x in a 30 m^3 indoor smog chamber, as well as the effect of SO_2 on SOA fromation with various inorganic seed particles.

2 Experimental section

2.1 Smog Chamber

The photooxidation experiments were performed in a 30 m^3 indoor smog chamber (4 m (height) × 2.5 m (width) × 3 m (length)), which was built in a temperature-controlled room located at the Research Center for Eco-Environment Sciences, Chinese Academy of Sciences (RCEES-CAS). Its schematic structure is shown in Fig. S1. Briefly, 120 UV lamps (365 nm, Philips TL 60/10R) were taken as the light source with a NO_2 photolysis rate of 0.55 min^{-1}, which was comparable to the irradiation intensity at noon in Beijing (Chou et al., 2011). A maglev fan installed at the bottom center of the smog chamber was used to mix sufficiently the introduced gas species and seed particles. Temperature (T) and relatively humidity (RH) in the chamber were (302 ±1) K and (39 ±1) %, respectively. Before each experiment, the chamber was flushed by purified dry zero air for ~36 h with a flow rate of 100 L min^{-1} until the particle number concentration in the chamber was lower than 20 cm^{-3}.

2.2 Experimental procedures

Gas-phase guaiacol was firstly introduced into the chamber by purified dry zero air flowing through the gently heated injector with a known volume of pure liquid guaiacol until guaiacol fully vaporized. Its concentration in the chamber was online monitored

by a high-resolution proton-transfer reaction time-of-flight mass spectrometer (HR-ToF-PTRMS) (Ionicon Analytik GmbH), and was calibrated by a commercial permeation tube (VICI AG INTERNATIONAL Valco Instruments Co., Inc.). When guaiacol concentration was stable, NO and SO_2 were introduced into the chamber by a mass flow meter using purified dry zero air as the carrier gas. Their concentrations were controlled by the injection time preset through the electromagnetic valve, and were measured by a NO_x analyzer (model 42i-TL, Thermo Fisher Scientific, Inc.) and a SO_2 analyzer (model 43i, Thermo Fisher Scientific Inc.), respectively. In this work, the initial ratio (V/V) of guaiacol concentration to NO_x concentration in the chamber was similar in all experiments (~1.2) (Tables 1 and 2). In addition, sodium chloride (NaCl) and ammonium sulfate ($(NH_4)_2SO_4$) were used as the inorganic seeds. The seed aerosols in the chamber were generated by the atomization of a 0.02 M aqueous solution. Through atomization, the size distribution of seed particles peaked at 51−58 nm was achieved, with a number concentration of 10100−11400 cm^{-3} (Table 2). After gas species and seed particles in the chamber were mixed well, the photooxidation experiment was carried out with the fan turned off. In this work, the OH concentrations in the chamber were (1.3−2.2) × 10^6 molecules cm^{-3}, calculated based on the degradation rate (7.53 × 10^{-11} cm^3 $molecule^{-1}$ s^{-1}) of guaiacol with OH radicals (Coeur-Tourneur et al., 2010a). The chemicals and gas samples used in this work were described in Supplement.

2.3 Data analysis

The HR-ToF-PTRMS with a time resolution of 1 min was used online to measure the gas phase concentration of guaiacol, and its m/z range was 10−500 in the process of data acquisition. Before data collection, the peaks of the protonated water ($[H_3{}^{18}O]^+$) and protonated acetone ($[C_3H_7O]^+$) ions at m/z 21.0246 and 59.0491 were used for mass calibration, with the aim to obtain accurate mass determination during experimental process. All data obtained by the HR-ToF-PTRMS were analyzed with the PTR-MS Viewer software (version 3.1.0, IONICON Analytik).

An Aerodyne high-resolution time-of-flight aerosol mass spectrometer (HR-ToF-AMS) was applied to online measure the chemical composition of particles and the non-refractory submicron aerosol mass (DeCarlo et al., 2006). For all experiments, the acquisition time of the HR-ToF-AMS was 2 min. The inlet flow rate, ionization efficiency, and particle sizing of the HR-ToF-AMS were calibrated at regular intervals, according to the standard protocols using the size-selected pure ammonium nitrate particles (Drewnick et al., 2005; Jimenez et al., 2003). All date obtained by the HR-ToF-AMS were analyzed by the ToF-AMS analysis toolkit SQUIRREL 1.57I/PIKA 1.16I version, in Igor Pro version 6.37. The size distribution and concentration of particles were monitored by a scanning mobility particle sizer (SMPS), which is composed of a differential mobility analyzer (DMA) (model 3082, TSI Inc.) and a condensation particle counter (CPC) (model 3776, TSI Inc.). Assuming that particles are spherical and non-porous, the average particle density could be calculated to be 1.4 g cm^{-3} using the equation $\rho=d_{va}/d_m$ (DeCarlo et al., 2004), where d_{va} is the mean vacuum

aerodynamic diameter measured by the HR-ToF-AMS and d_m is the mean volume-weighted mobility diameter measured by the SMPS. The mass concentration of particles measured by the HR-ToF-AMS was corrected by the SMPS data in this work using the same method as Gordon et al. (2014). In this work, the wall loss rate (k_{dep}) of $(NH_4)_2SO_4$ particles could be expressed as $k_{dep} = 4.15 \times 10^{-7} \times D_p^{1.89} + 1.39 \times D_p^{-0.88}$ (D_p is the particle diameter (nm)), which was measured according to the literature method (Takekawa et al., 2003) and was used to correct the wall loss of SOA. In addition, its wall loss rate was determined at predetermined time intervals, which only had a slight change among different experiments.

2.4 Vapor wall-loss correction

Previous studies have indicated that the losses of SOA-forming vapors to chamber wall can result in the substantial and systematic underestimation of SOA (Zhang et al., 2014, 2015). Therefore, SOA yields obtained in this work were also corrected by vapor wall loss. The effect of vapor wall deposition on SOA yields mainly depends on the competition between the uptake of organic vapors by aerosol particles and the chamber wall (Zhang et al., 2015). Thus, the ratio of the average gas-particle partitioning timescale ($\overline{\tau}_{g\text{-}p}$) over the course of experiment to the vapor wall deposition timescale ($\tau_{g\text{-}w}$) could be reasonably used to evaluate the underestimation of SOA yields. The detailed calculation of $\overline{\tau}_{g\text{-}p}$ and $\tau_{g\text{-}w}$ was shown in the Supplement.

3 Results and discussion

3.1 SOA yields

A series of experiments were conducted at different guaiacol/NO_x concentrations under atmospheric pressure. The experimental conditions and results are shown in Table 1. SOA yield was calculated to be the ratio of SOA mass concentration (M_o, μg m^{-3}) to the consumed guaiacol concentration (Δ[guaiacol], μg m^{-3}) at the end of each experiment (Kang et al., 2007). The results showed that SOA yield was dependent on the initial guaiacol concentration ($[Guaiacol]_0$). Higher precursor concentration would result in higher amount of condensable products, subsequently enhancing SOA formation (Lauraguais et al., 2012). In addition, it should be noted that SOA mass could directly affect the gas/particle partitioning via acting as the adsorption medium of oxidation products, thus higher SOA mass generally leads to higher SOA yield (Lauraguais et al., 2014b).

SOA yield (Y) could be represented by a widely-used semi-empirical model based on the absorptive gas-particle partitioning of semi-volatile products, typically calculated using the following equation (Odum et al., 1996):

$$Y = \sum_i M_o \frac{\alpha_i K_{om,i}}{1 + K_{om,i} M_o} \quad (1)$$

where α_i is the mass-based stoichiometric coefficient for the reaction producing the semi-volatile product i, $K_{om,i}$ is the gas-particle partitioning equilibrium constant, and M_o is the total aerosol mass concentration.

The yield curve for guaiacol photooxidation is shown in Fig. 1, obtained by plotting the SOA yield data in Table 1 according to Eq. (1). The yield data were accurately reproduced by a one-product model (R^2 = 0.97), while two or more products used in the

model did not significantly improve the fitting quality. The obtained values of α_i and $K_{om,i}$ for one-product model were (0.27 ±0.01) and (0.033 ±0.008) m^3 μg^{-1}, respectively. In previous studies, the one-product model was widely applied to describe SOA yields from the oxidation of aromatic compounds including methoxyphenols (Coeur-Tourneur et al., 2010b; Lauraguais et al., 2012, 2014b). In this work, this simulation suggests that the products in SOA have similar values of α_i and $K_{om,i}$, i.e., the obtained α_i and $K_{om,i}$ are the average values. The plot shown in Fig. S2 is the relationship between M_o versus Δ[guaiacol], of which slope (0.28) is slightly higher than α_i value (0.27). This suggests that the formed low-volatile products almost completely partitioned on the particle-phase according to the theoretical partition model (Lauraguais et al., 2012, 2014b).

In the previous studies, the significant SOA formation from the OH-initiated reaction of guaiacol has been reported (Lauraguais et al., 2014b; Yee et al., 2013). In this work, SOA yields for guaiacol photooxidation range from (9.46 ±1.71) % to (26.37 ± 2.83) %, shown in Table 1. According to the ratios of $\bar{\tau}_{g\text{-}p} / \tau_{g\text{-}w}$ (0.61−0.93), the determined SOA yields were underestimated by a factor of ~2 times, suggesting that vapor wall loss in the chamber could significantly affect SOA formation. The similar results were reported previously by Zhang et al. (2014), who indicated that SOA yields for toluene photooxidation were substantially underestimated by factors as much as 4 times, caused by vapor wall loss. As shown in Fig. 1, the vapor wall-loss corrected SOA yields were in the range of (15.24 ± 0.85) % to (50.89 ± 2.87) %, and could also be reproduced by a one-product model (R^2 = 0.96). This range overlaps SOA yields of

0.6 %−87 % for guaiacol oxidation under high NO_x condition (~10 ppmv NO), reported by Lauraguais et al. (2014b), using CH_3ONO as the OH source. Under low NO_x conditions (< 5 ppbv NO), SOA yields for guaiacol oxidation were in the range of 44 %−50 %, reported by Yee et al. (2013) using H_2O_2 as the OH source and $(NH_4)_2SO_4$ as seed particles; they also indicated that high NO_x concentration (> 200 ppbv NO) played an opposite role in SOA formation. Overall, the vapor wall-loss corrected SOA yields in this work are well in agreement with those reported previously (Lauraguais et al., 2014b; Yee et al., 2013), but the determined SOA yields are much lower. Therefore, the effect of vapor wall loss on SOA formation should be seriously taken into account.

In addition, the average N/C ratio of SOA for guaiacol photooxidation in the presence of NO_x is 0.037, calculated according to the element analysis by the HR-ToF-AMS. This indicates that NO_x incorporates in guaiacol photooxidation. This phenomenon is well supported by the previous studies, which have reported that the nitro-substituted products are the main products of the OH-initiated reaction of guaiacol in the presence of NO_x (Ahmad et al., 2017; Lauraguais et al., 2014b). The relative low volatility of these products could reasonably contribute to SOA formation (Duporté et al., 2016; Liu et al., 2016a). The average NO^+ / NO_2^+ ratio of SOA from guaiacol photooxidation is 4.08, which is higher than that (2.06−2.54) for ammonium nitrate, determined by the HR-ToF-AMS in this work. The possible explanation might be that nitro-organics and organonitrates both exist in SOA (Farmer et al., 2010; Sato et al., 2010). The relative abundance of organic N-containing compounds could be estimated

from the average N/C ratio. Assuming that the oxidation products in the SOA retain 7 carbon atoms, the yield of organic N-containing compounds is 25.9 %, which is the upper limit due to the possible C－C bond scission during photooxidation process.

3.2 Effect of SO_2 on SOA formation

3.2.1 SOA yields

In China, atmospheric SO_2 concentration is always in the range of several to dozens of ppbv, while in the severely polluted atmosphere it could be up to close 200 ppbv (Han et al., 2015; Li et al., 2017). In addition, a recent field measurement study has reported that the decrease of biogenic SOA mass concentration in the atmosphere has a positive correlation with SO_2 emission controls (Marais et al., 2017). Therefore, the effect of SO_2 at atmospheric levels on SOA formation from guaiacol photooxidation under atmospheric NO_x conditions was investigated. The experimental conditions and results are shown in Table 2. The formation of SOA, sulfate, and nitrate as a function of SO_2 concentration for guaiacol photooxidation is shown in Fig. S3, and the time-series variations in the concentrations of sulfate and nitrate are shown in Fig. S4. The decays of guaiacol, NO_x, and SO_2 are shown in Figs. S5a, S6a, and S7, respectively, which have the similar changing trends for different experiments. As illustrated in Fig. 2, the induction period became shorter with the increase of SO_2 concentration. The similar results caused by SO_2 have also been reported previously (Chu et al., 2016; Liu et al., 2016b). Meanwhile, M_o for the experiment without SO_2 (Exp. 1 in Table 2) increased from (63.62 ± 1.71) to (71.88 ± 1.43) and (78.59 ± 2.06) μg m^{-3}, enhanced by 12.98 %

and 23.53 %, respectively, when SO_2 concentration raised from 0 to 33 and 56 ppbv. The corresponding SOA yields were (21.60 ± 1.27) % and (23.42 ± 1.80) %, respectively. The similar results were reported by previous studies (Kleindienst et al., 2006; Lin et al., 2013; Liu et al., 2016b), which observed the significant enhancement of SOA yields for VOCs oxidation and the photochemical aging of gasoline vehicle exhaust in the presence of SO_2.

As shown in Fig. 3, $\bar{\tau}_{g\text{-}p} / \tau_{g\text{-}w}$ ratio decreased from 0.82 to 0.71 and 0.61 when SO_2 concentration increased from 0 to 33 and 56 ppbv. It suggests that the formed sulfate via SO_2 oxidation could serve as seed particles (Jaoui et al., 2008) and increase the surface areas of particles (Xu et al., 2016). These roles are favorable to partition more SOA-forming vapors onto particle phase (Zhang et al., 2014), consequently enhancing SOA yields. At the same time, as shown in Fig. S4 and Table 2, the sulfate concentration increased significantly from 7.42 to 17.89 μg m^{-3} when SO_2 concentration increased from 33 to 56 ppbv. Nevertheless, the particle peak attributed to sulfate formed via SO_2 oxidation was not observed by the SMPS during experimental process due to the quick particle growth in the presence of organic vapors. In this work, it is difficult to completely remove trace of NH_3 from zero air, thus the formed sulfate should be the mixture of H_2SO_4 and $(NH_4)_2SO_4$. The time-series changes in the concentration of ammonium salt at different SO_2 concentrations are shown in Fig. S8. Its concentration increased obviously with increasing SO_2 concentration, suggesting that the more amount of $(NH_4)_2SO_4$ was produced. The similar results have also been reported

recently by Chu et al. (2016). In addition, the surface area concentration of aerosol particles at the end time were calculated. As shown in Table 2, the final surface area of aerosol particles formed via guaiacol photooxidation increased from 1.25 $\times 10^3$ to 1.68 $\times 10^3$ and 2.04 $\times 10^3$ μm^2 cm^{-3} when SO_2 concentration increased from 0 to 33 and 56 ppbv. The increased surface area could be in favor of outcompeting the wall loss for low-volatility vapors produced from guaiacol photooxidation, i.e., more low-volatility vapors would be diverted from wall loss to the particles, consequently increasing SOA yields (Kroll et al., 2007). This is well supported by the decrease of $\bar{\tau}_{g\text{-}p} / \tau_{g\text{-}w}$ ratio with increasing SO_2 concentration, shown in Fig. 3.

The time-series changes in the mass concentrations of NO^+ and NO_2^+ are shown in Fig. S9a. The mass concentration of NO^+ increased more quickly than that of NO_2^+, and had a positive correlation with SO_2 concentration. But, compared to the experiment without SO_2, the presence of SO_2 had little impact on NO^+ / NO_2^+ and N/C ratios obtained at the end time, shown in Figs. S9b and S10b, respectively. These ratios indicated that organic N-containing compounds were also produced in this system (Farmer et al., 2010; Sato et al., 2010).

3.2.2 Oxidation state of SOA

The average carbon oxidation state (OS_C = 2O/C – H/C) of OA is widely used to represent the oxidation degree of atmospheric OA, because it takes into account the saturation level of carbon atoms in the OA (Kroll et al., 2011). As shown in Table 2, increasing SO_2 concentration (0−56 ppbv, Exps. 1−3) leads to the increase of OS_C

296 (0.11−0.18). The variations in H/C, O/C, and N/C ratios as a function of irradiation time
297 are shown in Fig. S10. In order to further identify the effect of SO_2 on the chemical
298 properties of SOA, positive matrix factorization (PMF) analysis for all AMS data
299 obtained at different SO_2 concentrations over the courses of experiments was carried
300 out. Two factors were obtained from the PMF analysis, and their mass spectra are shown
301 in Fig. 4. The organic mass fraction of m/z 44 (CO_2^+), named f_{44}, was 0.122 for Factor
302 2, which is higher than that (0.094) for Factor 1. Therefore, Factor 2 was tentatively
303 assigned to the more-oxidized SOA, while Factor 1 was the less-oxidized SOA (Ulbrich
304 et al., 2009). During the photooxidation process, these two factors had different
305 variations as a function of irradiation time. As shown in Fig. S11, Factor 1 increased
306 along with the reaction and then decreased, while Factor 2 had an increasing trend.
307 Compared to Exps. 1 and 2 in Table 2, the higher fraction of Factor 2 mass obtained at
308 56 ppbv SO_2 (Exp. 3 in Table 2) suggests that the formed SOA mainly consists of more-
309 oxidized products with relatively low volatility. This is well supported by the time-
310 series variations in the fraction of organic ion groups (CH^+, CHO^+, and CHO^+_{gt1}
311 (containing more than one oxygen atom)) (Fig. S12a), which shows the higher fraction
312 of CHO^+_{gt1} and lower fraction of CH^+ obtained at higher SO_2 concentration,
313 consequently resulting in higher OS_C of SOA.

314 Previous studies mostly reported that the enhancement of SOA yield in the presence
315 of SO_2 was ascribed to the functionalization and oligomerization reactions (Cao and
316 Jang, 2007; Jaoui et al., 2008 ; Liu et al., 2016b; Xu et al., 2016). If the oligomerization

317 reaction plays a predominant role in the presence of SO_2 which will lead to particle
318 phase H_2SO_4, the carbon number of oligomers will increase but their net O/C or H/C
319 values have little change, consequently resulting in little change in the oxidation state
320 of SOA (Chen et al., 2011). Nevertheless, we observed that SO_2 not only enhanced SOA
321 yields, but also resulted in higher OS_C (Table 2 and Fig. 5). This suggests that the
322 functionalization reaction might be predominant with SO_2, which leads to higher OS_C
323 of products with low molecular weight (MW) (Ye et al., 2018), consequently resulting
324 in an overall increase in OS_C and SOA yields. More recently, Ye et al. (2018) also found
325 the similar results in the ozonolysis of limonene. Fig. S13 shows the differences among
326 the normalized mass spectra of SOA formed at different SO_2 concentrations. As shown
327 in Fig. S13a, the signal fractions from the low-MW species were enhanced significantly
328 in the presence of SO_2, and were much higher than those from the high-MW species
329 ($m/z > 300$). The similar results were also observed in Fig. S13b when increasing SO_2
330 concentration. In other words, SO_2 played a more important role in the formation of
331 organic S-containing compounds and the formation or uptake of low-MW species,
332 compared to the formation of high-MW species (i.e., oligomers) that should be
333 reasonably produced via the acid-catalyzed heterogeneous reactions (Cao and Jang,
334 2007; Jaoui et al., 2008; Liu et al., 2016b; Xu et al., 2016).

335 In this work, assuming that all organic S-containing compounds are organosulfates
336 and have the same response factor and fragmentation as methyl sulfate, the conservative
337 lower-bound concentration of organosulfates was calculated to be in the range of (2.1

338 ± 0.8) to (4.3 ± 1.7) ng m^{-3} using the method described by Huang et al. (2015) shown
339 in the Supplement, and increased with the increase of SO_2 concentration. This
340 concentration range is close to those derived from the atmospheric oxidation of
341 polycyclic aromatic hydrocarbons and alkane (Meade et al., 2016; Riva et al., 2015).
342 Fig. S14 is the examples of the ions (i.e., CSO^+, $CH_3SO_2^+$, and $CH_3SO_3^+$) of methyl
343 sulfate obtained at 56 ppbv SO_2 (Exp. 3 in Table 2). On the other hand, sulfuric acid
344 formed from SO_2 may be favorable for the uptake of water-soluble low-MW species
345 (e.g., small carboxylic acids and aldehydes) and also be helpful to retain them in aerosol
346 phase, which would result in the increase of OS_C. This is well supported by the time-
347 series variations in the concentrations of acetic acid at different SO_2 concentrations
348 measured by the HR-ToF-PTRMS (Fig. S15a), which shows that acetic acid
349 concentration decreased with the increase of SO_2 concentration (0−56 ppbv). These
350 results were in good agreement with those reported by Liggio et al. (2005) and Liu et
351 al. (2010), who observed that the uptake of organic compounds under acidic conditions
352 would be enhanced significantly. Recently, Huang et al. (2016) have also reported that
353 acetic acid is present in SOA formed via α-pinene ozonolysis and its uptake would
354 increase in the presence of seed particles. In addition, Krapf et al. (2016) have indicated
355 that peroxides in SOA are unstable and liable to decompose into volatile compounds,
356 consequently leading to decrease SOA yield and OS_C. But, Ye et al. (2018) found that
357 the reactions of SO_2 with organic peroxides were the dominant sink of SO_2, initiated by
358 the heterogeneous uptake of SO_2 under humidity condition. These reactions would

result in the formation of organic S-containing compounds, consequently increasing SOA yields and OS_C.

3.3 Effect of inorganic seed particles on SOA formation

Seed particle is one of the critical factors influencing SOA formation (Ge et al., 2017a), thus the effects of inorganic seeds (i.e., NaCl and $(NH_4)_2SO_4$) on SOA formation from guaiacol photooxidation were investigated. As shown in Fig. 6, the presence of inorganic seed particles could accelerate SOA growth rate at the initial stage of photooxidation (i.e., shorten induction period), followed by the decrease of growth rate along with the reaction, because the presence of inorganic seeds could promote the condensation of SOA-forming organic products and consequently increase SOA formation (Yee et al., 2013). The results showed that M_o for the experiment without seed particles (Exp. 1 in Table 2) increased from (63.62 ± 1.71) to (79.44 ± 1.86) and (84.91 ± 2.01) μg m^{-3} (Table 2), enhanced by 24.87 % and 33.46 %, respectively, with $(NH_4)_2SO_4$ and NaCl seed particles. The corresponding SOA yields were (23.31 ± 1.59) % and (24.54 ± 1.73) %, respectively. In previous work, the similar results about the enhancements of SOA formation by NaCl and $(NH_4)_2SO_4$ seed particles were reported in the oxidation of VOCs (Ge et al., 2017a, 2017b; Huang et al., 2013, 2017). As shown in Fig. 3, $\bar{\tau}_{g\text{-}p} / \tau_{g\text{-}w}$ ratios with $(NH_4)_2SO_4$ and NaCl seed particles were 0.62 and 0.54, respectively, which suggested that more SOA-forming vapors were partitioned onto particle phase in the presence of NaCl seed particles (Zhang et al., 2014), consequently resulting in relatively higher SOA yield.

As shown in Table 2 and Fig. 6, the SOA mass concentration in the presence of NaCl seed particles was higher than that in the presence of $(NH_4)_2SO_4$ seed particles. In addition, OS_C of SOA in the presence of NaCl seed particles is 0.29, slightly higher than that (0.20) in the presence of $(NH_4)_2SO_4$ seed particles. Recently, it has been also reported that the presence of $(NH_4)_2SO_4$ and $NaNO_3$ seed particles could enhance significantly the oxidation state of SOA, compared to without seed particles (Huang et al., 2016). In this work, the experimental conditions for seed experiments are almost the same (Table 2), including reactant concentration, temperature, RH, and the number and diameter of seed particles. Therefore, the differences in the yield and oxidation state of SOA were reasonably resulted from the different chemical compositions of SOA in the presence of different inorganic seeds. As shown in Figs. S12b and S12c, compared to $(NH_4)_2SO_4$ seed particles, the higher fraction of CHO^+_{gt1} and lower fraction of CH^+ were obtained with NaCl seed particles, consequently resulting in higher OS_C of SOA. The time-series evolution of O/C, H/C, and N/C ratios is shown in Figs. S16 and S17, which indicate that O/C ratios (0.94−0.99) with NaCl seed particles at the end of experiments are higher than those (0.90−0.93) with $(NH_4)_2SO_4$ seed particles. Fig. 7 shows the mass spectra of SOA in the presence of NaCl and $(NH_4)_2SO_4$ seed particles obtained by the HR-ToF-AMS, as well as their difference mass spectrum. As shown in Fig. 7, f_{44} for SOA in the presence of NaCl seed particles was higher than that obtained in the presence of $(NH_4)_2SO_4$ seed particles, while the mass fractions of m/z 15 (CH_3) and 29 (CHO) fragments were both lower. The m/z 44 ion (CO^+_2) is mainly contributed

401 from acids or acid-derived species, such as esters (Ng et al., 2011). The higher f_{44} of
402 SOA with NaCl than $(NH_4)_2SO_4$ seed particles suggests that the distribution of highly
403 oxidized small carboxylic acids onto seed particles plays an important role in SOA
404 formation, consequently resulting in higher oxidation state of SOA (Huang et al., 2016;
405 Ng et al., 2011). Compared to $(NH_4)_2SO_4$, the hygroscopicity of NaCl is stronger (Ge
406 et al., 2017a; Gysel et al., 2002). The molar ratio of H_2O to NaCl is about 0.1 at 40 %
407 RH, and water is mainly adsorbed on NaCl particles (Weis and Ewing, 1999). Thus, the
408 greater water content on the particle surface could facilitate the uptake of highly
409 oxidized small carboxylic acids onto NaCl particles, which might explain the higher
410 SOA oxidation state observed in the presence of NaCl seed particles (Huang et al.,
411 2016). As shown in Fig. S15, the concentration of acetic acid in the gas phase with
412 NaCl seed particles was lower than that with $(NH_4)_2SO_4$ seed particles. It suggests that
413 the uptake of acetic acid on NaCl seed particles might be higher than that on $(NH_4)_2SO_4$
414 seed particles under the similar experimental conditions (i.e., NO_x and guaiacol
415 concentrations, temperature, and RH). Moreover, the adsorbed acid products would also
416 generate H^+ ions, which could catalyze heterogeneous reactions to produce more-
417 oxidized products or oligomers with relatively low volatility (Fig. S18), consequently
418 resulting in the enhancement of SOA formation (Huang et al., 2013, 2017; Cao and
419 Jang, 2007; Jaoui et al., 2008; Liu et al., 2016b; Xu et al., 2016).

420 In addition, the possible formation of Cl atoms from the photolysis of nitryl
421 chloride ($ClNO_2 \xrightarrow{h\nu} Cl + NO_2$, k_1 = ~10^{-4} s^{-1}) (Mielke et al., 2011) and the reaction

of OH radical with Cl^- ($Cl^- + OH \rightarrow Cl + OH^-$, k_2 = ~10^9 M^{-1} s^{-1}) (Fang et al., 2014) would also initiate a series of reactions to oxidize SOA composition, which might be another reason for higher OS_C observed with NaCl seed particles. According to the rate constant (10^9 M^{-1} s^{-1}) (Fang et al., 2014), the uptake coefficient (3.4×10^{-3}) of OH radicals on NaCl particles (Park et al., 2008), and the concentrations of OH radicals and Cl^-, the concentration of Cl atoms produced from the reaction of OH radical with Cl^- was estimated to be less than 38 molecules cm^{-3}, which was much higher than that from the photolysis of $ClNO_2$ due to the slow photolysis rate constant of ~10^{-4} s^{-1} (Mielke et al., 2011). Compared to OH concentration in the chamber, the oxidation of SOA composition by Cl atoms should be insignificant.

3.4 Synergetic effect of SO_2 and inorganic seed particles on SOA formation

According to the former results obtained in this work, it is clearly known that SO_2 and inorganic seed particles both have a positive role in enhancing SOA formation. Therefore, their possible synergetic effects on SOA formation were investigated. Considering the experiments performed under the comparable conditions (Table 2), the results should be reasonably reliable. The decays of guaiacol, NO_x, and SO_2 are shown in Figs. S5, S6, and S7, respectively, which have the similar changing trends for different experiments. Fig. S19 shows the time-series evolution in the sulfate concentration in the presence of different SO_2 concentrations and seed particles, which indicates that sulfate concentration is dependent on SO_2 concentration. As shown in Fig. 8, the addition of SO_2 into the chamber in the presence of inorganic seed particles

443 significantly promoted SOA formation from guaiacol photooxidation, but had an
444 ignorable impact on the induction period. When SO_2 concentration raised from 0 to 30
445 and 54 ppbv in the presence of NaCl seed particles, M_o increased from (84.91 ± 2.01)
446 to (90.89 ± 2.28) and (98.86 ± 2.11) μg m^{-3}, enhanced by 7.04 % and 16.43 %,
447 respectively, and the corresponding SOA yields were (26.78 ± 1.97) % and (29.06 ±
448 1.82) %. For $(NH_4)_2SO_4$ seed particles, M_o increased from (79.44 ± 1.86) to (84.35 ±
449 2.09) for 33 ppbv SO_2 and (89.92 ± 2.31) μg m^{-3} for 54 ppbv SO_2, enhanced by 6.18 %
450 and 13.19 %, respectively, and the corresponding SOA yields were (24.58 ± 1.78) %
451 and (26.37 ± 1.98) %. As shown in Fig. 3, $\bar{\tau}_{g\text{-}p} / \tau_{g\text{-}w}$ ratio had a decreasing trend when
452 increasing SO_2 concentration in the presence of seed particles, suggesting that the
453 underestimation of SOA yields caused by vapor wall loss was weakened significantly
454 because of the additional sulfate formed from SO_2 oxidation. Thus, inorganic seed
455 particles and SO_2 have a synergestic effect on SOA formation.

456 As shown in Table 2 and Fig. 5, it should be noted that OS_C of SOA increased in
457 the presence of SO_2, which was well supported by the time-series variations in H/C,
458 O/C, and N/C ratios at different SO_2 concentrations with NaCl and $(NH_4)_2SO_4$ as seed
459 particles, shown in Figs. S16 and S17. In addition, as shown in Figs. S12b and S12c,
460 the higher fraction of CHO^+_{gt1} and lower fraction of CH^+ were obtained at higher SO_2
461 concentration, consequently resulting in higher OS_C of SOA. Fig. S20 shows the mass
462 spectra of SOA with NaCl and $(NH_4)_2SO_4$ as seed particles at different SO_2
463 concentrations obtained by the HR-ToF-AMS. As illustrated in Fig. S20, SO_2 addition

was in favor of increasing the value of f_{44}, suggesting that more products with higher OS_C are produced by the functionalization reaction (Ye et al., 2018). Meanwhile, Table 2 shows that the final surface area of aerosol particles increased in the presence of SO_2, which played a positive role in diverting more low-volatility vapors from wall loss to the particles, consequently enhancing SOA yields (Kroll et al., 2007). In addition, the presence of inorganic seeds could promote the condensation of SOA-forming organic products and the heterogeneous uptake of SO_2 (Yee et al., 2013), providing favorable conditions for the following reactions. Meanwhile, the higher hygroscopicity of NaCl than $(NH_4)_2SO_4$ might be helpful to dissolve more acid substances on NaCl particle surface (e.g., H_2SO_4 and organic acid), especially in the presence of SO_2. This hypothesis could be supported by the variations in acetic acid concentration in the presence of different seed particles and SO_2 concentrations (Fig. S15), which shows that acetic acid concentration decreased with the increase of SO_2 concentration (0−54 ppbv). The dissolved acid compounds might be helpful to catalyze heterogeneous reactions (Cao and Jang, 2007; Huang et al., 2013, 2017; Jaoui et al., 2008; Liu et al., 2016b; Xu et al., 2016). Figs. S21 and S22 show the differences among the normalized mass spectra of SOA formed at different SO_2 concentrations with various seed particles. The results indicated that the signal fractions from the low-MW species increased significantly in the presence of SO_2, and were much higher than those from the high-MW species (m/z > 300). Compared to Exps. 2 and 3 in Table 2 with no seed particles, the conservative lower-bound concentrations of organosulfates formed with seed

particles were similar and in the range of (2.2 ± 0.7) to (4.6 ± 1.8) ng m^{-3}, which might be caused by the similar SO_2 concentrations applied for experiments. With NaCl and $(NH_4)_2SO_4$ as seed particles, SOA yields and OS_C both increased with the increase of SO_2, suggesting that the functionalization reaction should be more dominant than oligomerization reaction during photooxidation process.

4 Conclusions and atmospheric implications

In this work, SOA formation from guaiacol photooxidation in the presence of NO_x was investigated in a 30 m^3 smog chamber. SOA yields for guaiacol photooxidation were in the range of (9.46 ± 1.71) % to (26.37 ± 2.83) %, and could be expressed well by a one-product model. These yields were underestimated by a factor of ~2 times according to $\bar{\tau}_{g\text{-}p} / \tau_{g\text{-}w}$ ratios. The presence of SO_2 could increase SOA yield and OS_C, indicating that the functionalization reaction should be more dominant than oligomerization reaction. Meanwhile, the similar effect of SO_2 was also observed with NaCl and $(NH_4)_2SO_4$ seed particles. But, SOA yield and OS_C in the presence of NaCl seed particles were both slightly higher than those in the presence of $(NH_4)_2SO_4$ seed particles. In addition, the results indicated the synergetic contribution of SO_2 and inorganic seed particles to SOA formation. The decreasing trend of $\bar{\tau}_{g\text{-}p} / \tau_{g\text{-}w}$ ratio in the presence of seed particles and SO_2 suggested that more SOA-forming vapors were partitioned onto particle phase, consequently increasing SOA yields. The average N/C ratio (0.037) of SOA suggested that NO_x participated in the process of guaiacol photooxidation, resulting in the formation of organic N-containing compounds.

The significant SOA formation from guaiacol photooxidation at the atmospheric levels of SO_2 and NO_x in this work suggests that it should pay more attention to the SOA formation from biomass burning and its subsequent effects on haze evolution, especially in China with nationwide biomass burning, because recent studies have indicated that SOA formed from biomass burning plays an important role in haze pollution in China (Ding et al., 2017; Li et al., 2017). In addition, the results imply that the oxidation of SO_2 and VOCs should be tightly combined, and SO_2 has a direct impact on the physics and chemistry of SOA formation. Although guaiacol concentrations in the chamber study are higher than those in the ambient atmosphere, the results obtained in this work could provide new information for SOA formation from the photooxidation of methoxyphenols, and might be useful for SOA modeling, especially for air quality simulation modeling of the specific regions experiencing serious pollution caused by fine particulate matter. In addition, the results would help to further understand the photochemical aging process of smoke plumes from biomass burning in the atmosphere.

Data availability

The experimental data are available upon request to the corresponding authors.

Author contributions

CL, TC, YL, and HH designed the research and wrote the paper. CL, TC, and JL performed the experiments. CL, TC, YL, JL, HH, and PZ carried out the data analysis. All authors contributed to the final paper.

Competing interests

The authors declare that they have no conflict of interest.

Acknowledgements

This work was financially supported by the National Key R&D Program of China (2016YFC0202700), the National Natural Science Foundation of China (21607088 and 41877306), China Postdoctoral Science Foundation funded project (2017M620071), the Applied Basic Research Project of Science and Technology Department of Sichuan Province (2018JY0303) and Key Research Program of Frontier Sciences, CAS (QYZDB-SSW-DQC018). Liu Y. would like to thank Beijing University of Chemical Technology for financial supporting. Authors would also acknowledge the experimental help provided by Dr. Xiaolei Bao from Hebei Provincial Academy of Environmental Sciences, Shijiazhuang, China.

References

Ahmad, W., Coeur, C., Tomas, A., Fagniez, T., Brubach, J.-B., and Cuisset, A.: Infrared spectroscopy of secondary organic aerosol precursors and investigation of the hygroscopicity of SOA formed from the OH reaction with guaiacol and syringol, Appl. Opt., 56, E116-E122, https://doi.org/10.1364/ao.56.00e116, 2017.

Bari, M. A., and Kindzierski, W. B.: Fine particulate matter (PM2.5) in Edmonton, Canada: Source apportionment and potential risk for human health, Environ. Pollut., 218, 219-229, https://doi.org/10.1016/j.envpol.2016.06.014, 2016.

Cao, G., and Jang, M.: Effects of particle acidity and UV light on secondary organic aerosol formation from oxidation of aromatics in the absence of NO_x, Atmos. Environ., 41, 7603-7613, https://doi.org/10.1016/j.atmosenv.2007.05.034, 2007.

Chen, Q., Liu, Y., Donahue, N. M., Shilling, J. E., and Martin S. T.: Particle-phase chemistry of secondary organic material: Modeled compared to measured O:C and H:C elemental ratios provide constraints, Environ. Sci. Technol., 45, 4763-4770, https://doi.org/10.1021/es104398s, 2011.

Chen, Y., and Bond, T. C.: Light absorption by organic carbon from wood combustion, Atmos. Chem. Phys., 10, 1773-1787, https://doi.org/10.5194/acp-10-1773-2010, 2010.

Chou, C. C. K., Tsai, C. Y., Chang, C. C., Lin, P. H., Liu, S. C., and Zhu, T.: Photochemical production of ozone in Beijing during the 2008 Olympic Games, Atmos. Chem. Phys., 11, 9825-9837, https://doi.org/10.5194/acp-11-9825-2011, 2011.

Chu, B., Zhang, X., Liu, Y., He, H., Sun, Y., Jiang, J., Li, J., and Hao, J.: Synergetic formation of secondary inorganic and organic aerosol: Effect of SO_2 and NH_3 on particle formation and growth, Atmos. Chem. Phys., 16, 14219-14230, https://doi.org/10.5194/acp-16-14219-2016, 2016.

Chu, B., Liggio, J., Liu, Y., He, H., Takekawa, H., Li, S.-M., and Hao, J.: Influence of metal-mediated aerosol-phase oxidation on secondary organic aerosol formation from the ozonolysis and OH-oxidation of α-pinene, Sci. Rep., 7, 40311, https://doi.org/10.1038/srep40311, 2017.

Coeur-Tourneur, C., Cassez, A., and Wenger, J. C.: Rate coefficients for the gas-phase reaction of hydroxyl radicals with 2-methoxyphenol (guaiacol) and related compounds, J. Phys. Chem. A, 114, 11645-11650, https://doi.org/10.1021/jp1071023, 2010a.

Coeur-Tourneur, C., Foulon, V., and Lareal, M.: Determination of aerosol yields from 3-methylcatechol and 4-methylcatechol ozonolysis in a simulation chamber, Atmos. Environ., 44, 852-857, https://doi.org/10.1016/j.atmosenv.2009.11.027, 2010b.

DeCarlo, P. F., Slowik, J. G., Worsnop, D. R., Davidovits, P., and Jimenez, J. L.: Particle morphology and density characterization by combined mobility and aerodynamic diameter measurements. Part 1: Theory, Aerosol Sci. Technol., 38, 1185-1205, https://doi.org/10.1080/027868290903907, 2004.

DeCarlo, P. F., Kimmel, J. R., Trimborn, A., Northway, M. J., Jayne, J. T., Aiken, A. C., Gonin, M., Fuhrer, K., Horvath, T., Docherty, K. S., Worsnop, D. R., and Jimenez, J. L.: Field-deployable, high-resolution, time-of-flight aerosol mass spectrometer, Anal. Chem., 78, 8281-8289, https://doi.org/10.1021/ac061249n, 2006.

Ding, X., Zhang, Y.-Q., He, Q.-F., Yu, Q.-Q., Wang, J.-Q., Shen, R.-Q., Song, W., Wang, Y.-S., and Wang, X.-M.: Significant increase of aromatics-derived secondary organic aerosol during fall to winter in China, Environ. Sci. Technol., 51, 7432-7441, https://doi.org/10.1021/acs.est.6b06408, 2017.

Drewnick, F., Hings, S. S., DeCarlo, P., Jayne, J. T., Gonin, M., Fuhrer, K., Weimer, S., Jimenez, J. L., Demerjian, K. L., Borrmann, S., and Worsnop, D. R.: A new time-of-flight aerosol mass spectrometer (TOF-AMS)-instrument description and first field deployment, Aerosol Sci. Technol., 39, 637-658, https://doi.org/10.1080/02786820500182040, 2005.

Dupont, G., Parshintsev, J., Barreira, L. M. F., Hartonen, K., Kulmala, M., and Riekkola, M.-L.: Nitrogen-containing low volatile compounds from

pinonaldehyde-dimethylamine reaction in the atmosphere: A laboratory and field study, Environ. Sci. Technol., 50, 4693-4700, https://doi.org/10.1021/acs.est.6b00270, 2016.
El Zein, A., Coeur, C., Obeid, E., Lauraguais, A., and Fagniez, T.: Reaction kinetics of catechol (1,2-benzenediol) and guaiacol (2-methoxyphenol) with ozone, J. Phys. Chem. A, 119, 6759-6765, https://doi.org/10.1021/acs.jpca.5b00174, 2015.
Fang, J., Fu, Y., and Shang, C.: The roles of reactive species in micropollutant degradation in the UV/free chlorine system, Environ. Sci. Technol., 48, 1859-1868, https://doi.org/10.1021/es4036094, 2014.
Farmer, D. K., Matsunaga, A., Docherty, K. S., Surratt, J. D., Seinfeld, J. H., Ziemann, P. J., and Jimenez, J. L.: Response of an aerosol mass spectrometer to organonitrates and organosulfates and implications for atmospheric chemistry, Proc. Natl. Acad. Sci. U. S. A., 107, 6670-6675, https://doi.org/10.1073/pnas.0912340107, 2010.
Ge, S., Xu, Y., and Jia, L.: Effects of inorganic seeds on secondary organic aerosol formation from photochemical oxidation of acetone in a chamber, Atmos. Environ., 170, 205-215, https://doi.org/10.1016/j.atmosenv.2017.09.036, 2017a.
Ge, S., Xu, Y., and Jia, L.: Secondary organic aerosol formation from propylene irradiations in a chamber study, Atmos. Environ., 157, 146-155, https://doi.org/10.1016/j.atmosenv.2017.03.019, 2017b.
Gordon, T. D., Presto, A. A., Nguyen, N. T., Robertson, W. H., Na, K., Sahay, K. N., Zhang, M., Maddox, C., Rieger, P., Chattopadhyay, S., Maldonado, H., Maricq, M. M., and Robinson, A. L.: Secondary organic aerosol production from diesel vehicle exhaust: impact of aftertreatment, fuel chemistry and driving cycle, Atmos. Chem. Phys., 14, 4643-4659, https://doi.org/10.5194/acp-14-4643-2014, 2014.
Gysel, M., Weingartner, E., and Baltensperger, U.: Hygroscopicity of aerosol particles at low temperatures. 2. Theoretical and experimental hygroscopic properties of laboratory generated aerosols, Environ. Sci. Technol., 36, 63-68, https://doi.org/10.1021/es010055g, 2002.
Han, T., Liu, X., Zhang, Y., Qu, Y., Zeng, L., Hu, M., and Zhu, T.: Role of secondary aerosols in haze formation in summer in the Megacity Beijing, J. Environ. Sci., 31, 51-60, https://doi.org/10.1016/j.jes.2014.08.026, 2015.
Hawthorne, S. B., Krieger, M. S., Miller, D. J., and Mathiason, M. B.: Collection and quantitation of methoxylated phenol tracers for atmospheric pollution from residential wood stoves, Environ. Sci. Technol., 23, 470-475, https://doi.org/10.1021/es00181a013, 1989.
Hawthorne, S. B., Miller, D. J., Langenfeld, J. J., and Krieger, M. S.: PM10 high-volume collection and quantitation of semivolatile and nonvolatile phenols, methoxylated phenols, alkanes, and polycyclic aromatic hydrocarbons from winter urban air and their relationship to wood smoke emissions, Environ. Sci. Technol., 26, 2251-2262, https://doi.org/10.1021/es00035a026, 1992.
Huang, D. D., Li, Y. J., Lee, B. P., and Chan, C. K.: Analysis of organic sulfur

compounds in atmospheric aerosols at the HKUST supersite in Hong Kong using HR-ToF-AMS, Environ. Sci. Technol., 49, 3672-3679, https://doi.org/10.1021/es5056269, 2015.

Huang, D. D., Zhang, X., Dalleska, N. F., Lignell, H., Coggon, M. M., Chan, C.-M., Flagan, R. C., Seinfeld, J. H., and Chan, C. K.: A note on the effects of inorganic seed aerosol on the oxidation state of secondary organic aerosol-alpha-Pinene ozonolysis, J. Geophys. Res.-Atmos., 121, 12476-12483, https://doi.org/10.1002/2016jd025999, 2016.

Huang, M., Hao, L., Gu, X., Hu, C., Zhao, W., Wang, Z., Fang, L., and Zhang, W.: Effects of inorganic seed aerosols on the growth and chemical composition of secondary organic aerosol formed from OH-initiated oxidation of toluene, J. Atmos. Chem., 70, 151-164, https://doi.org/10.1007/s10874-013-9262-9, 2013.

Huang, M., Hao, L., Cai, S., Gu, X., Zhang, W., Hu, C., Wang, Z., Fang, L., and Zhang, W.: Effects of inorganic seed aerosols on the particulate products of aged 1,3,5-trimethylbenzene secondary organic aerosol, Atmos. Environ., 152, 490-502, https://doi.org/10.1016/j.atmosenv.2017.01.010, 2017.

Jaoui, M., Edney, E. O., Kleindienst, T. E., Lewandowski, M., Offenberg, J. H., Surratt, J. D., and Seinfeld, J. H.: Formation of secondary organic aerosol from irradiated α-pinene/toluene/NO_x mixtures and the effect of isoprene and sulfur dioxide, J. Geophys. Res.-Atmos., 113, D09303, https://doi.org/10.1029/2007jd009426, 2008.

Jimenez, J. L., Jayne, J. T., Shi, Q., Kolb, C. E., Worsnop, D. R., Yourshaw, I., Seinfeld, J. H., Flagan, R. C., Zhang, X., Smith, K. A., Morris, J. W., and Davidovits, P.: Ambient aerosol sampling using the Aerodyne Aerosol Mass Spectrometer, J. Geophys. Res.-Atmos., 108, 8425, https://doi.org/10.1029/2001JD001213, 2003.

Kang, E., Root, M. J., Toohey, D. W., and Brune, W. H.: Introducing the concept of Potential Aerosol Mass (PAM), Atmos. Chem. Phys., 7, 5727-5744, https://doi.org/10.5194/acp-7-5727-2007, 2007.

Kleindienst, T. E., Edney, E. O., Lewandowski, M., Offenberg, J. H., and Jaoui, M.: Secondary organic carbon and aerosol yields from the irradiations of isoprene and α-pinene in the presence of NO_x and SO_2, Environ. Sci. Technol., 40, 3807-3812, https://doi.org/10.1021/es052446r, 2006.

Krapf, M., El Haddad, I., Bruns, E. A., Molteni, U., Daellenbach, K. R., Prevot, A. S. H., Baltensperger, U., and Dommen, J.: Labile peroxides in secondary organic aerosol, Chem, 1, 603-616, https://doi.org/10.1016/j.chempr.2016.09.007, 2016.

Kroll, J. H., Chan, A. W. H., Ng, N. L., Flagan, R. C., andSeinfeld, J. H.: Reactions of semivolatile organics and their effects on secondary organic aerosol formation, Environ. Sci. Technol., 41, 3545-3550, https://doi.org/10.1021/es062059x, 2007.

Kroll, J. H., Donahue, N. M., Jimenez, J. L., Kessler, S. H., Canagaratna, M. R., Wilson, K. R., Altieri, K. E., Mazzoleni, L. R., Wozniak, A. S., Bluhm, H., Mysak, E. R., Smith, J. D., Kolb, C. E., and Worsnop, D. R.: Carbon oxidation state as a metric for describing the chemistry of atmospheric organic aerosol, Nature Chem., 3, 133-139, https://doi.org/10.1038/nchem.948, 2011.

679 Lauraguais, A., Coeur-Tourneur, C., Cassez, A., and Seydi, A.: Rate constant and
680 secondary organic aerosol yields for the gas-phase reaction of hydroxyl radicals
681 with syringol (2,6-dimethoxyphenol), Atmos. Environ., 55, 43-48,
682 https://doi.org/10.1016/j.atmosenv.2012.02.027, 2012.
683 Lauraguais, A., Bejan, I., Barnes, I., Wiesen, P., Coeur-Tourneur, C., and Cassez, A.:
684 Rate coefficients for the gas-phase reaction of chlorine atoms with a series of
685 methoxylated aromatic compounds, J. Phys. Chem. A, 118, 1777-1784,
686 https://doi.org/10.1021/jp4114877, 2014a.
687 Lauraguais, A., Coeur-Tourneur, C., Cassez, A., Deboudt, K., Fourmentin, M., and
688 Choel, M.: Atmospheric reactivity of hydroxyl radicals with guaiacol (2-
689 methoxyphenol), a biomass burning emitted compound: Secondary organic
690 aerosol formation and gas-phase oxidation products, Atmos. Environ., 86, 155-
691 163, https://doi.org/10.1016/j.atmosenv.2013.11.074, 2014b.
692 Lauraguais, A., El Zein, A., Coeur, C., Obeid, E., Cassez, A., Rayez, M.-T., and Rayez,
693 J.-C.: Kinetic study of the gas-phase reactions of nitrate radicals with
694 methoxyphenol compounds: Experimental and theoretical approaches, J. Phys.
695 Chem. A, 120, 2691-2699, https://doi.org/10.1021/acs.jpca.6b02729, 2016.
696 Lelieveld, J., Crutzen, P. J., Ramanathan, V., Andreae, M. O., Brenninkmeijer, C. A. M.,
697 Campos, T., Cass, G. R., Dickerson, R. R., Fischer, H., de Gouw, J. A., Hansel, A.,
698 Jefferson, A., Kley, D., de Laat, A. T. J., Lal, S., Lawrence, M. G., Lobert, J. M.,
699 Mayol-Bracero, O. L., Mitra, A. P., Novakov, T., Oltmans, S. J., Prather, K. A.,
700 Reiner, T., Rodhe, H., Scheeren, H. A., Sikka, D., and Williams, J.: The Indian
701 Ocean Experiment: Widespread air pollution from South and Southeast Asia,
702 Science, 291, 1031-1036, https://doi.org/10.1126/science.1057103, 2001.
703 Li, H., Zhang, Q., Zhang, Q., Chen, C., Wang, L., Wei, Z., Zhou, S., Parworth, C.,
704 Zheng, B., Canonaco, F., Prevot, A. S. H., Chen, P., Zhang, H., Wallington, T. J.,
705 and He, K.: Wintertime aerosol chemistry and haze evolution in an extremely
706 polluted city of the North China Plain: Significant contribution from coal and
707 biomass combustion, Atmos. Chem. Phys., 17, 4751-4768,
708 https://doi.org/10.5194/acp-17-4751-2017, 2017.
709 Liggio, J., Li, S.-M., and McLaren, R.: Reactive uptake of glyoxal by particulate matter,
710 J. Geophys. Res.-Atmos., 110, D10304, https://doi.org/10.1029/2004JD005113,
711 2005.
712 Lin, Y. H., Knipping, E. M., Edgerton, E. S., Shaw, S. L., and Surratt, J. D.:
713 Investigating the influences of SO_2 and NH_3 levels on isoprene-derived secondary
714 organic aerosol formation using conditional sampling approaches, Atmos. Chem.
715 Phys., 13, 8457–8470, https://doi.org/10.5194/acp-13-8457-2013, 2013.
716 Liu, J., Lin, P., Laskin, A., Laskin, J., Kathmann, S. M., Wise, M., Caylor, R., Imholt,
717 F., Selimovic, V., and Shilling, J. E.: Optical properties and aging of light-
718 absorbing secondary organic aerosol, Atmos. Chem. Phys., 16, 12815-12827,
719 https://doi.org/10.5194/acp-16-12815-2016, 2016a.
720 Liu, T., Wang, X., Hu, Q., Deng, W., Zhang, Y., Ding, X., Fu, X., Bernard, F., Zhang,

Z., Lu, S., He, Q., Bi, X., Chen, J., Sun, Y., Yu, J., Peng, P., Sheng, G., and Fu, J.: Formation of secondary aerosols from gasoline vehicle exhaust when mixing with SO_2, Atmos. Chem. Phys., 16, 675-689, https://doi.org/10.5194/acp-16-675-2016, 2016b.

Liu, Z., Ge, M., Yin, S., and Wang, W.: Uptake and reaction kinetics of α-pinene and β-pinene with sulfuric acid solutions, Chem. Phys. Lett., 491, 146-150, https://doi.org/10.1016/j.cplett.2010.04.004, 2010.

Marais, E. A., Jacob, D. J., Turner, J. R., and Mickley, L. J.: Evidence of 1991-2013 decrease of biogenic secondary organic aerosol in response to SO_2 emission controls, Environ. Res. Lett., 12, 054018, https://doi.org/10.1088/1748-9326/aa69c8, 2017.

Meade, L. E., Riva, M., Blomberg, M. Z., Brock, A. K., Qualters, E. M., Siejack, R. A., Ramakrishnan, K., Surratt, J. D., and Kautzman, K. E.: Seasonal variations of fine particulate organosulfates derived from biogenic and anthropogenic hydrocarbons in the mid-Atlantic United States, Atmos. Environ., 145, 405-414, https://doi.org/10.1016/j.atmosenv.2016.09.028, 2016.

Mielke, L. H., Furgeson, A., and Osthoff, H. D.: Observation of $ClNO_2$ in a mid-continental urban environment, Environ. Sci. Technol., 45, 8889-8896, https://doi.org/10.1021/es201955u, 2011.

Naeher, L. P., Brauer, M., Lipsett, M., Zelikoff, J. T., Simpson, C. D., Koenig, J. Q., and Smith, K. R.: Woodsmoke health effects: A review, Inhal. Toxicol., 19, 67-106, https://doi.org/10.1080/08958370600985875, 2007.

Ng, N. L., Chhabra, P. S., Chan, A. W. H., Surratt, J. D., Kroll, J. H., Kwan, A. J., McCabe, D. C., Wennberg, P. O., Sorooshian, A., Murphy, S. M., Dalleska, N. F., Flagan, R. C., and Seinfeld, J. H.: Effect of NO_x level on secondary organic aerosol (SOA) formation from the photooxidation of terpenes, Atmos. Chem. Phys., 7, 5159-5174, https://doi.org/10.5194/acp-7-5159-2007, 2007.

Ng, N. L., Canagaratna, M. R., Jimenez, J. L., Chhabra, P. S., Seinfeld, J. H., and Worsnop, D. R.: Changes in organic aerosol composition with aging inferred from aerosol mass spectra, Atmos. Chem. Phys., 11, 6465-6474, https://doi.org/10.5194/acp-11-6465-2011, 2011.

Nolte, C. G., Schauer, J. J., Cass, G. R., and Simoneit, B. R. T.: Highly polar organic compounds present in wood smoke and in the ambient atmosphere, Environ. Sci. Technol., 35, 1912-1919, https://doi.org/10.1021/es001420r, 2001.

O'Neill, E. M., Kawam, A. Z., Van Ry, D. A., and Hinrichs, R. Z.: Ozonolysis of surface-adsorbed methoxyphenols: kinetics of aromatic ring cleavage vs. alkene side-chain oxidation, Atmos. Chem. Phys., 14, 47-60, https://doi.org/10.5194/acp-14-47-2014, 2014.

Odum, J. R., Hoffmann, T., Bowman, F., Collins, D., Flagan, R. C., and Seinfeld, J. H.: Gas/particle partitioning and secondary organic aerosol yields, Environ. Sci. Technol., 30, 2580-2585, https://doi.org/10.1021/es950943+, 1996.

Park, J.-H., Ivanov, A. V., and Molina, M. J.: Effect of relative humidity on OH uptake

by surfaces of atmospheric importance, J. Phys. Chem. A, 112, 6968-6977, https://doi.org/10.1021/jp8012317, 2008.

Riva, M., Tomaz, So, Cui, T., Lin, Y. H., Perraudin, E., Gold, A., Stone, E. A., Villenave, E., and Surratt, J. D.: Evidence for an unrecognized secondary anthropogenic source of organosulfates and sulfonates: Gas-phase oxidation of polycyclic aromatic hydrocarbons in the presence of sulfate aerosol, Environ. Sci. Technol., 49, 6654−6664, https://doi.org/10.1021/acs.est.5b00836, 2015.

Sarrafzadeh, M., Wildt, J., Pullinen, I., Springer, M., Kleist, E., Tillmann, R., Schmitt, S. H., Wu, C., Mentel, T. F., Zhao, D., Hastie, D. R., and Kiendler-Scharr, A.: Impact of NO_x and OH on secondary organic aerosol formation from beta-pinene photooxidation, Atmos. Chem. Phys., 16, 11237-11248, https://doi.org/10.5194/acp-16-11237-2016, 2016.

Sato, K., Takami, A., Isozaki, T., Hikida, T., Shimono, A., and Imamura, T.: Mass spectrometric study of secondary organic aerosol formed from the photo-oxidation of aromatic hydrocarbons, Atmos. Environ., 44, 1080-1087, https://doi.org/10.1016/j.atmosenv.2009.12.013, 2010.

Schauer, J. J., Kleeman, M. J., Cass, G. R., and Simoneit, B. R. T.: Measurement of emissions from air pollution sources. 3. C-1-C-29 organic compounds from fireplace combustion of wood, Environ. Sci. Technol., 35, 1716-1728, https://doi.org/10.1021/es001331e, 2001.

Simoneit, B. R. T., Rogge, W. F., Mazurek, M. A., Standley, L. J., Hildemann, L. M., and Cass, G. R.: Lignin pyrolysis products, lignans, and resin acid as specific tracers of plant classes in emissions from biomass combustion, Environ. Sci. Technol., 27, 2533-2541, https://doi.org/10.1021/es00048a034, 1993.

Takekawa, H., Minoura, H., and Yamazaki, S.: Temperature dependence of secondary organic aerosol formation by photo-oxidation of hydrocarbons, Atmos. Environ., 37, 3413-3424, https://doi.org/10.1016/s1352-2310(03)00359-5, 2003.

Ulbrich, I. M., Canagaratna, M. R., Zhang, Q., Worsnop, D. R., and Jimenez, J. L.: Interpretation of organic components from Positive Matrix Factorization of aerosol mass spectrometric data, Atmos. Chem. Phys., 9, 2891-2918, https://doi.org/10.5194/acp-9-2891-2009, 2009.

Weis, D. D., and Ewing, G. E.: Water content and morphology of sodium chloride aerosol particles, J. Geophys. Res.-Atmos., 104, 21275-21285, https://doi.org/10.1029/1999jd900286, 1999.

Xu, L., Middlebrook, A. M., Liao, J., de Gouw, J. A., Guo, H., Weber, R. J., Nenes, A., Lopez-Hilfiker, F. D., Lee, B. H., Thornton, J. A., Brock, C. A., Neuman, J. A., Nowak, J. B., Pollack, I. B., Welti, A., Graus, M., Warneke, C., and Ng, N. L.: Enhanced formation of isoprene-derived organic aerosol in sulfur-rich power plant plumes during Southeast Nexus, J. Geophys. Res.-Atmos., 121, 11137-11153, https://doi.org/10.1002/2016jd025156, 2016.

Yang, B., Zhang, H., Wang, Y., Zhang, P., Shu, J., Sun, W., and Ma, P.: Experimental and theoretical studies on gas-phase reactions of NO_3 radicals with three

methoxyphenols: Guaiacol, creosol, and syringol, Atmos. Environ., 125, 243-251, https://doi.org/10.1016/j.atmosenv.2015.11.028, 2016.

Ye, J., Abbatt, J. P. D., and Chan, A. W. H.: Novel pathway of SO_2 oxidation in the atmosphere: reactions with monoterpene ozonolysis intermediates and secondary organic aerosol, Atmos. Chem. Phys., 18, 5549-5565, https://doi.org/10.5194/acp-18-5549-2018, 2018.

Yee, L. D., Kautzman, K. E., Loza, C. L., Schilling, K. A., Coggon, M. M., Chhabra, P. S., Chan, M. N., Chan, A. W. H., Hersey, S. P., Crounse, J. D., Wennberg, P. O., Flagan, R. C., and Seinfeld, J. H.: Secondary organic aerosol formation from biomass burning intermediates: Phenol and methoxyphenols, Atmos. Chem. Phys., 13, 8019-8043, https://doi.org/10.5194/acp-13-8019-2013, 2013.

Zhang, X., Cappa, C. D., Jathar, S. H., McVay, R. C., Ensberg, J. J., Kleeman, M. J., and Seinfeld, J. H.: Influence of vapor wall loss in laboratory chambers on yields of secondary organic aerosol, Proc. Natl. Acad. Sci. U. S. A., 111, 5802-5807, https://doi.org/10.1073/pnas.1404727111, 2014.

Zhang, X., Schwantes, R. H., McVay, R. C., Lignell, H., Coggon, M. M., Flagan, R. C., and Seinfeld, J. H.: Vapor wall deposition in Teflon chambers, Atmos. Chem. Phys., 15, 4197-4214, https://doi.org/10.5194/acp-15-4197-2015, 2015.

Table 1. Experimental conditions and results for guaiacol photoxidation in the presence NO_x.

Exp.	$[Guaiacol]_0$ ($\mu g\ m^{-3}$)	$\triangle$[Guaiacol] ($\mu g\ m^{-3}$)[a]	$[NO_x]_0$ (ppbv)	$[NO]_0$ (ppbv)	RH (%)	T (K)	M_o ($\mu g\ m^{-3}$)[b]	Yield (%)
1	136.83	112.34	25.1	13.2	39	302	10.63 ± 0.65	9.46 ± 1.71
2	309.06	282.33	52.7	34.4	38	302	34.72 ± 0.94	12.30 ± 0.98
3	375.19	335.94	58.3	44.5	40	302	63.62 ± 1.71	18.94 ± 1.49
4	718.49	613.25	116.7	98.5	38	302	130.19 ± 3.28	21.23 ± 1.56
5	1321.25	1116.20	209.2	184.1	39	302	256.88 ± 6.69	23.01 ± 1.75
6	1470.66	1175.03	248	200	38	302	297.65 ± 8.85	25.33 ± 2.21
7	2197.36	1664.29	335	286	38	302	438.82 ± 10.25	26.37 ± 2.83

[a] The consumed guaiacol concentration at the end of each experiment.

[b] M_o is the mass concentration of SOA.

827 **Table 2.** Experimental conditions and results for guaiacol photoxidation in the presence of seed particles and SO_2.

Exp.	$[Guaiacol]_0$ ($\mu g\ m^{-3}$)	$\triangle$[Guaiacol] ($\mu g\ m^{-3}$)[a]	Seed	$[SO_2]_0$ (ppbv)	$[NO_x]_0$ (ppbv)	$[NO]_0$ (ppbv)	RH (%)	T (K)	N_S (m^{-3})[b]	D_S (nm)[c]	C_{seed} ($\mu g\ m^{-3}$)[d]	$C_{sulfate}$ ($\mu g\ m^{-3}$)[e]	S_0 ($\mu m^2\ cm^{-3}$)[f]	S_f ($\mu m^2\ cm^{-3}$)[g]	$\bar{\tau}_{g\text{-}p} / \tau_{g\text{-}w}$ [h]	M_o ($\mu g\ m^{-3}$)[i]	Yield (%)	OS_C[j]
1	375.19	335.94	–	–	58.3	44.5	40	302	–	–	–	–	–	1.25×10^3	0.82	63.62 ± 1.71	18.94 ± 1.49	0.11 ± 0.007
2	363.53	332.79	–	33	54.5	37.4	38	302	–	–	–	7.42	–	1.68×10^3	0.71	71.88 ± 1.43	21.60 ± 1.27	0.14 ± 0.006
3	370.12	335.58	–	56	57.3	41.8	38	302	–	–	–	17.89	–	2.04×10^3	0.61	78.59 ± 2.06	23.42 ± 1.80	0.18 ± 0.006
4	379.05	346.03	NaCl	–	58.8	40.7	39	302	10700	56	15.63	–	2.69×10^2	1.47×10^3	0.54	84.91 ± 2.01	24.54 ± 1.73	0.29 ± 0.007
5	378.44	339.34	NaCl	30	57.4	41.9	38	302	11300	58	13.84	7.51	2.64×10^2	2.32×10^3	0.43	90.89 ± 2.28	26.78 ± 1.97	0.30 ± 0.008
6	380.77	340.15	NaCl	54	60.1	46.1	39	301	11200	56	14.28	16.67	2.81×10^2	2.91×10^3	0.35	98.86 ± 2.11	29.06 ± 1.82	0.33 ± 0.008
7	373.57	340.86	$(NH_4)_2SO_4$	–	58.3	42.6	39	302	10400	53	15.45	–	2.75×10^2	1.53×10^3	0.62	79.44 ± 1.86	23.31 ± 1.59	0.20 ± 0.006
8	376.26	343.19	$(NH_4)_2SO_4$	33	56.8	38.9	38	302	10100	53	14.38	7.84	2.80×10^2	2.57×10^3	0.53	84.35 ± 2.09	24.58 ± 1.78	0.22 ± 0.007
9	381.33	341.01	$(NH_4)_2SO_4$	54	57.8	39.2	38	303	10700	51	14.90	17.25	2.82×10^2	3.10×10^3	0.44	89.92 ± 2.31	26.37 ± 1.98	0.23 ± 0.004

828 [a] The consumed guaiacol concentration at the end of each experiment. [b] N_S is the initial seed number. [c] D_S is the average diameter of seed particles.

829 [d] C_{seed} is the initial concentration of seed. [e] $C_{sulfate}$ is the sulfate concentration formed by SO_2 oxidation. [f] The initial surface area of seed particles.

830 [g] The final surface area of aerosol particles (seed + organic aerosol), measured by the SMPS. [h] The ratio of the average gas-particle partitioning

831 timescale ($\bar{\tau}_{g\text{-}p}$) over the course of experiment to the vapor wall deposition timescale ($\tau_{g\text{-}w}$). [i] M_o is the mass concentration of SOA. [j] OS_C is the

832 average oxidation state of carbon of SOA.

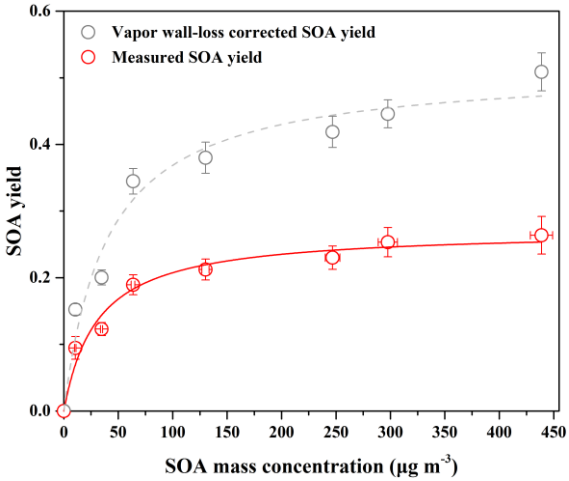

Figure 1. SOA yield as a function of SOA mass concentration (M_o) for guaiacol photooxidation in the presence of NO_x at different guaiacol concentrations. The lines were fit to the experimental data using a one-product model. Values of α and $K_{om,i}$ used to generate the solid line were (0.27 ± 0.01) and (0.033 ± 0.008), and their values for the dot line were (0.52 ± 0.03) and (0.025 ± 0.006), respectively.

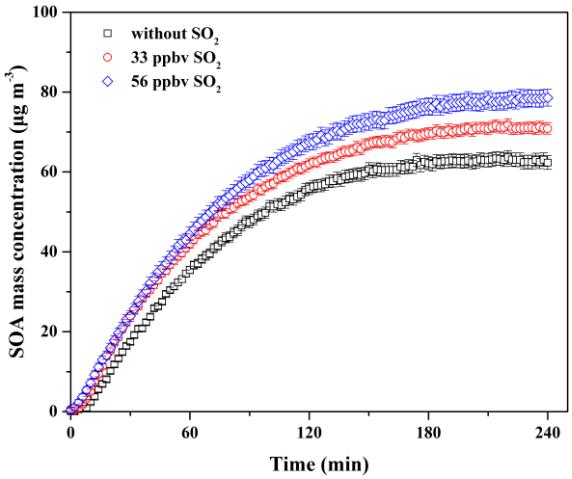

839

840 **Figure 2.** Time-dependent growth curves of SOA mass concentration for guaiacol

841 photooxidation at different SO_2 levels (Exps. 1−3 in Table 2).

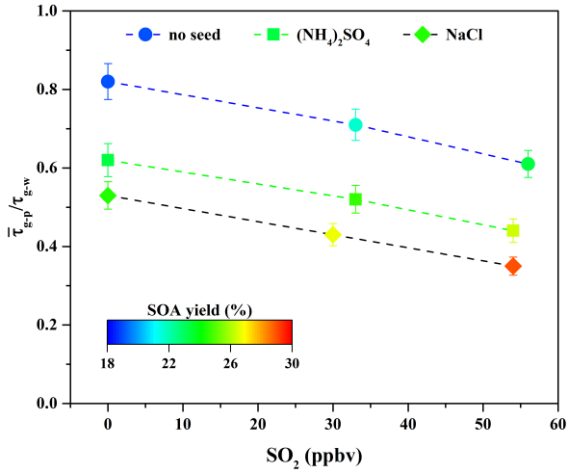

842

843 **Figure 3.** Variations in $\overline{\tau}_{g\text{-}p} / \tau_{g\text{-}w}$ ratio in the presence of various seed particles as a

844 function of SO_2 concentration.

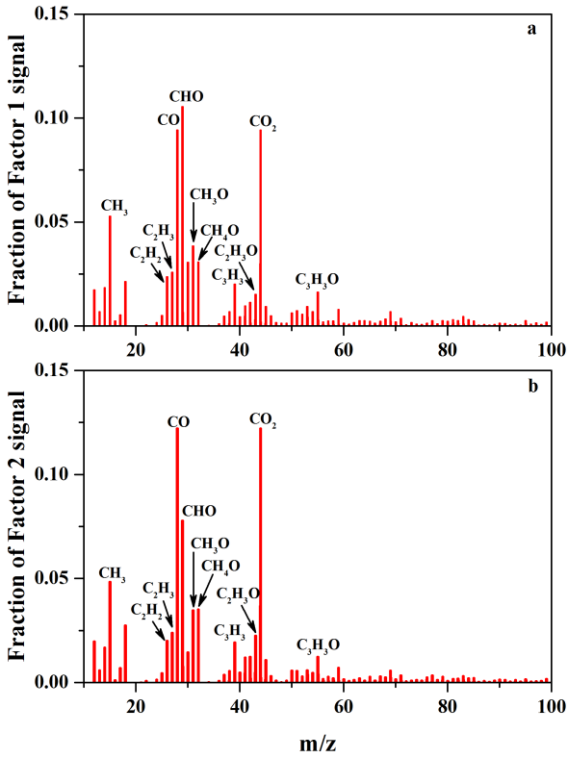

Figure 4. Mass spectra of Factor 1 (a) and Factor 2 (b) for the formed SOA identified by applying PMF analysis to the AMS data, obtained at different SO_2 concentrations over the courses of experiments.

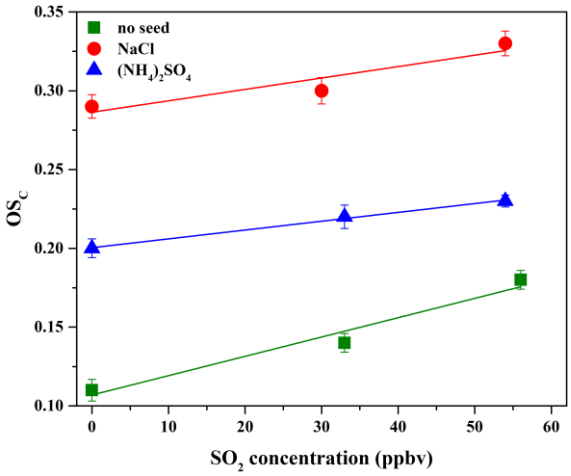

Figure 5. OS_C of SOA formed in the presence of various seed particles as a function of SO_2 concentration.

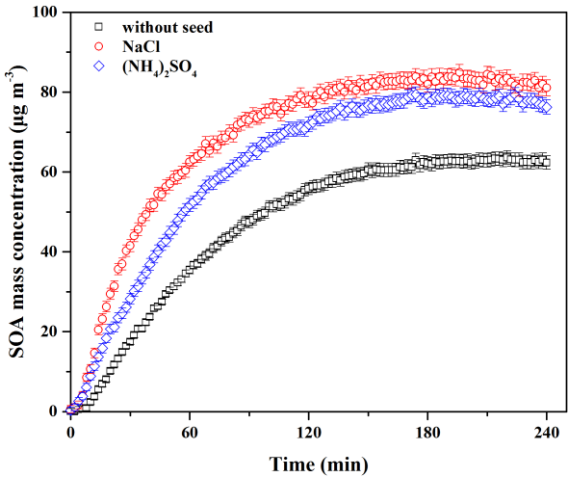

852

853 **Figure 6.** Time-dependent growth curves of SOA mass concentration for guaiacol

854 photooxidation in the presence of inorganic seed particles (Exps. 1, 4 and 7 in Table 2).

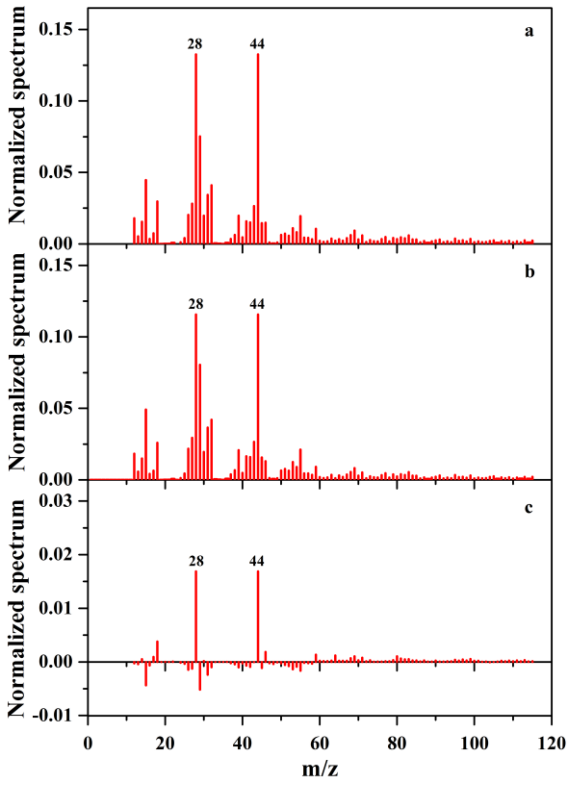

855

856 **Figure 7.** Mass spectra of SOA with NaCl (a) and $(NH_4)_2SO_4$ (b) as seed particles

857 obtained by the HR-ToF-AMS, as well as their difference mass spectrum (c) obtained

858 by a minus b.

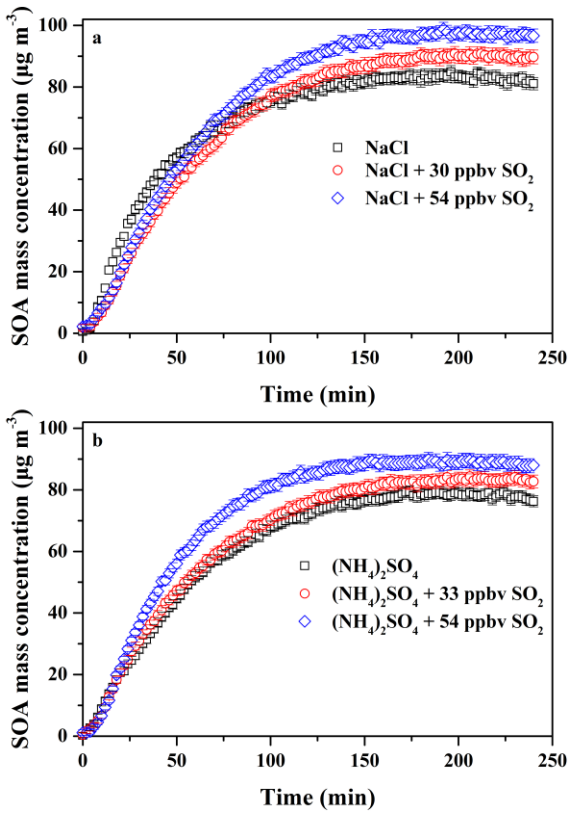

859

860 **Figure 8.** Time-dependent growth curves of SOA mass concentration for guaiacol

861 photooxidation in the presence of SO_2 and inorganic seed particles (a: NaCl; b:

862 $(NH_4)_2SO_4$) (Exps. 4−9 in Table 2).